Geometric Optimization of Electrically Coupled Liquid Metal Manifolds for WCLL Blankets

Leo Bühler and Chiara Mistrangelo

***Abstract*— A number of previous theoretical and experimental studies for helium-cooled or water-cooled lead lithium (WCLL) blankets show that the major fraction of magnetohydrodynamic (MHD) pressure drop in the breeder flow originates from manifolds that distribute and collect the liquid metal into and from the breeder units (BUs). Moreover, those studies revealed that without a proper design of the manifolds, the flow partitioning among breeder units would be strongly nonuniform along the poloidal direction. In the present work, MHD flows in electrically coupled liquid metal manifolds are studied by using an efficient hybrid model that has been developed for prediction of MHD pressure drop in such geometries and for determining flow distribution in BUs. The tool combines global mass conservation and pressure drop correlations with detailed 3-D simulations. From the experience gained when applying the model to the geometry of a test blanket module (TBM), it is concluded that the design of the manifolds requires optimization for achieving a balanced flow partitioning among BUs. In the second step, the hybrid model is applied to determine the optimum position of the baffle plates that separate the feeding and collecting ducts in manifolds in order to guarantee comparable flow rates in all BUs.**

***Index Terms*— Liquid metal blankets, magnetohydrodynamics (MHDs), pressure drop and flow distribution.**

I. Introduction

IN THE frame of the European fusion research program, liquid metal blankets are being developed and experimentally tested in the International Thermonuclear Experimental Reactor (ITER), where lead lithium (PbLi) is used as breeder material and heat transfer medium. The present European reference concept is a water-cooled lead lithium (WCLL) blanket, where liquid metal velocities in the columnar arranged breeder units (BUs) are very small [1]. For purification and tritium extraction, the liquid metal is circulated toward external ancillary facilities. When the electrically conducting PbLi moves through the plasma-confining magnetic field, magnetohydrodynamics (MHD) affects the flow distribution and may create a huge pressure drop. Moreover, leakage currents across conducting walls electrically couple neighboring fluid regions.

Manifolds distributing PbLi among BUs are key components for the performance of blanket modules since the major fraction of pressure drop arises in these elements [2]. Their design eventually determines the liquid metal flow partitioning in BUs [3]. For a reasonable performance of the blanket system, it is required that each BU receives sufficient fresh PbLi in order to avoid local accumulation of tritium. Therefore a good understanding of the flow partitioning in BUs and pressure drop in the blanket system is required. The problem of homogeneous flow distribution from manifolds to breeder channels represents a challenge also for applications in other blanket types as discussed for instance for dual coolant blankets in [5], [6], and [7].

Liquid metal flows in manifolds designed for a test blanket module (TBM) for ITER [8] are analyzed by using a hybrid approach, where 3-D simulations for electrically coupled prototypical elements are combined with global mass conservation and pressure balancing for the entire blanket module [9]. Deficiencies in BU flow partitioning for the present TBM design are emphasized and a proposal is made for optimal positions of the baffle plates that separate feeding and draining manifolds, based on simulation results. As an example, the present analysis focuses on the liquid metal flow in a scaled experimental mock-up of one column of BUs [10], which has been derived according to the available ITER TBM design [11] (see Fig. 1).

II. Mathematical Model

Although the mathematical model has been described in detail in [9], major ideas are outlined in the following since they form the basis for a full understanding of the concept of optimization of the manifold geometry as outlined below in the present article. The model couples the flow in the manifolds with the flow in BUs and allows calculating the flow partitioning among BUs.

For notation, the subscripts f, d, and BU denote in the following feeding and draining manifolds, and BUs (see Fig. 1).

The TBM mock-up consists of $1 \le i \le N = 8$ BUs of poloidal length dx. For simplicity, the exchange of fluid via BU_i is assumed to happen at the same poloidal position x_i. The analysis is based on the nondimensional coordinate ξ, that measures geometric dimensions in fractions of the poloidal length L

$$x = L\,\xi,\ 0 < \xi < 1. \tag{1}$$

Cross sections of feeding and draining manifolds A_f and A_d are part of the entire manifold cross section $A = A_f + A_d$ and the cross section A_{BU} is a typical cross section in a BU.

Manuscript received 29 July 2023; revised 22 January 2024; accepted 1 February 2024. This work was supported by the Framework of the EUROfusion Consortium, funded by the European Union via the Euratom Research and Training Program under Grant 101052200—EUROfusion. The review of this article was arranged by Senior Editor R. Chapman. *(Corresponding author: Leo Bühler.)*

The authors are with the Karlsruhe Institute of Technology, 76021 Karlsruhe, Germany (e-mail: leo.buehler@kit.edu; chiara.mistrangelo@kit.edu).

Color versions of one or more figures in this article are available at https://doi.org/10.1109/TPS.2024.3362689.

Digital Object Identifier 10.1109/TPS.2024.3362689

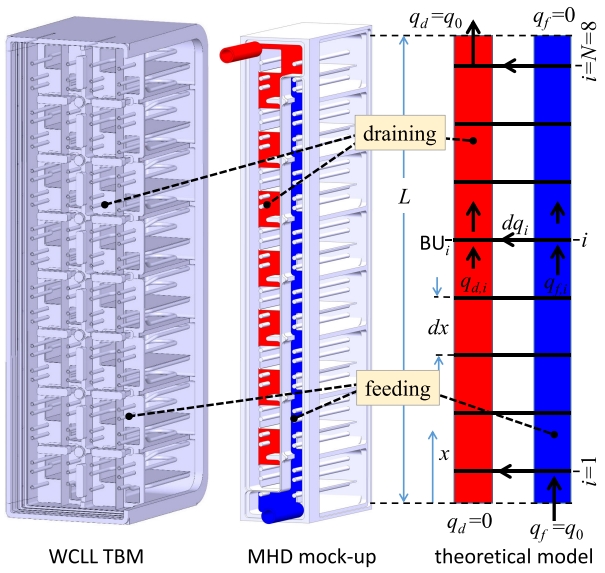

Fig. 1. Design of a scaled mock-up for experiments in MEKKA with 8 BUs arranged along the poloidal direction [10]. The geometry has been derived from the WCLL ITER TBM as proposed, e.g., in [8]. View into the system of manifolds and principle sketch defining details of the theoretical model.

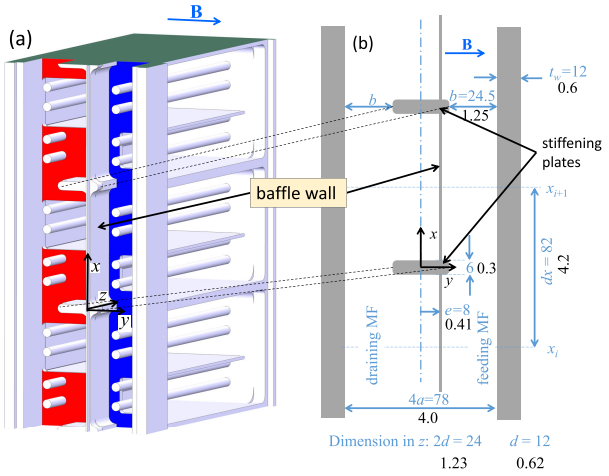

Fig. 2. (a) Three-dimensional view of a TBM mock-up with manifolds and BUs used for MHD model experiments in the MEKKA facility at KIT [10], derived from ITER TBM design [8]. (b) Geometry, dimensions and coordinate system in feeding and draining manifolds. Black notation is nondimensional and scaled with a, blue one is dimensional and measured in mm.

The flow rates in feeding and draining manifolds $q_f = q_0\alpha_f$ and $q_d = q_0\alpha_d$ are measured as fractions α_f and α_d of the total volume flux q_0. The unit BU$_i$ exchanges a fraction $dq_i = q_0\, d\alpha_i$ between feeding and draining manifold at poloidal position x_i (see sketch in Fig. 1). After passing position x_i the flow rate fractions in feeding and draining manifolds become

$$\alpha_{f,i+1} = \alpha_{f,i} - d\alpha_i,\ \ \alpha_{d,i+1} = \alpha_{d,i} + d\alpha_i \tag{2}$$

where mass conservation for incompressible fluids requires

$$\alpha_{f,i} + \alpha_{d,i} = 1 \text{ and } \sum_{i=1}^{N} d\alpha_i = 1. \tag{3}$$

With the pressure scale $p_0 = a\,\sigma B^2 u_M$ and definition of a nondimensional pressure $\pi = p/p_0$ we find pressure variations along manifolds

$$\pi_{f,i+1} = \pi_{f,i} - \Delta p_{f,i}\left(\alpha_{f,i}\right) \tag{4}$$

$$\pi_{d,i+1} = \pi_{d,i} - \Delta p_{d,i}\left(\alpha_{d,i}\right) \tag{5}$$

depending on flow rate fractions α. Here, $\Delta p_{f,i}$ and $\Delta p_{d,i}$ denote nondimensional pressure drops in coupled element i of feeding and draining manifold. The average Hartmann length in manifolds is a (see Fig. 2 for geometric details) and the mean velocity in manifolds is defined as $u_M = q_0/A$.

From the pressure drop along a BU (where Δp_{BU} denotes pressure drop in one BU with flow rate q_0, scaled by p_0)

$$\pi_{f,i} - \pi_{d,i} = d\alpha_i\, \Delta p_{\mathrm{BU}} \tag{6}$$

it is possible to determine the nondimensional flow rates in BUs as

$$d\alpha_i = \left(\pi_{f,i} - \pi_{d,i}\right)/\Delta p_{\mathrm{BU}}. \tag{7}$$

Solutions are obtained by an iterative procedure starting with an initial guess of $d\alpha_i$ satisfying the mass balance (3) from which the flow rate distributions in manifolds follows according to (2). Then the pressure distributions in feeding and draining manifolds are determined using (4) and (5), assuming $\pi_{f,0} = 0$ as the reference pressure. The yet unknown initial value $\pi_{d,0}$ is determined using mass conservation (3). Iterations with under-relaxation are repeated until converged solutions for pressure and flow rates are achieved (see also [9]).

III. Analysis for Current TBM Design

A. Numerical Model for Manifold Elements

For evaluation of (4) and (5) it is necessary to know $\Delta p_{f,i}\left(\alpha_{f,i}\right)$ and $\Delta p_{d,i}\left(\alpha_{d,i}\right)$ depending on their respective flow partitioning $\alpha_{f,i}$ and $\alpha_{d,i}$. Geometric details are as described in [9] but repeated here for completeness and reproducibility. According to the design shown in Fig. 1, the manifold cross sections are constant along the poloidal x-direction but they have periodical constrictions originating from stiffening plates that penetrate the manifold region (see Fig. 2). Manifolds are separated from each other by the common so-called baffle wall across which both channels are electrically coupled. The dimensions of the present example are taken from a scaled mock-up for MHD experiments in the MEKKA facility of KIT, where a representative manifold element has dimensions dx (82 mm) $\times$ 4a (78 mm) $\times$ 2d (24 mm). Details are shown in Fig. 2(b) and in [10]. In the current design, the manifold baffle wall is shifted by a distance e (8 mm) with respect to the symmetry plane $y = 0$. The analysis for the manifolds is simplified in the sense that all walls are treated with an average thickness of $t_w = 12$ mm except the manifold baffle wall whose thickness is only 2 mm.

The importance of electromagnetic forces compared to viscous forces is characterized in the simulations by the manifold Hartmann number

$$Ha = aB\sqrt{\frac{\sigma}{\rho\nu}} \tag{8}$$

where B denotes the strength of the magnetic field. Thermophysical properties are those of the model fluid NaK

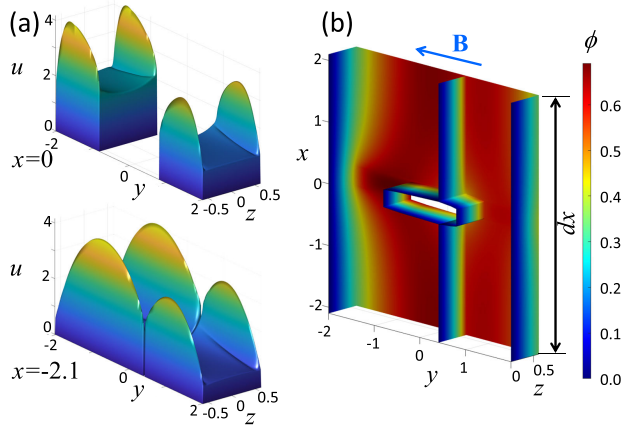

Fig. 3. Results of a simulation with electromagnetic coupling, with pressure differences $\Delta p_d = \Delta p_f = 0.562$. (a) Velocity profiles in the symmetry plane $x = 0$ and near the entrance $x = -2.1$ and (b) view on the distribution of nondimensional electric potential on the fluid-wall interface in half of the geometry for $z > 0$.

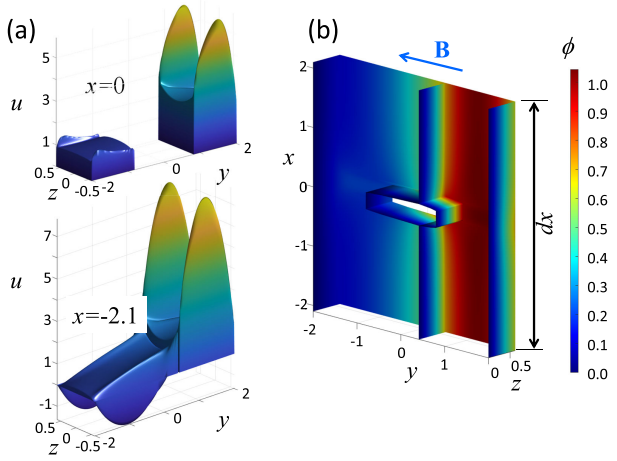

Fig. 4. Results of a simulation with electromagnetic coupling with no driving pressure difference in the draining manifold $\Delta p_d = 0$. (a) Velocity profiles in the symmetry plane $x = 0$ and near the entrance $x = -2.1$ and (b) view on the distribution of nondimensional electric potential on the fluid-wall interface in half of the geometry for $z > 0$.

foreseen in MEKKA experiments where $\rho = 863\,\mathrm{kg/m^3}$, $\nu = 9.02 \cdot 10^{-7}\,\mathrm{m^2/s}$, $\sigma = 2.79 \cdot 10^6\,1/\Omega\mathrm{m}$ [12]. The conductivity of the mock-up walls is $\sigma_w = 1.24 \cdot 10^6\,1/\Omega\mathrm{m}$ [13] which leads to wall conductance ratios for external walls $c = t_w\sigma_w/a\sigma = 0.274$ and $c = 0.046$ for the manifold baffle walls. The electrically coupled 3-D analysis of a fraction i of the manifold is performed analogous to [14] using asymptotic methods described in [15] and it is complementary to [9], where the separating wall was placed for first analyses at $y = e = 0$. In the asymptotic analysis the flow is driven by applied (arbitrarily chosen) driving pressure differences $\Delta p'_f$ and $\Delta p'_d$ yielding flow rate fractions α'_f and α'_d. Since the asymptotic analysis is linear, it is then possible to scale the solution for all variables by a constant factor such that mass conservation (3) is satisfied, i.e., $\alpha_f + \alpha_d = 1$ and Δp_f and Δp_d are obtained as shown, e.g., in Fig. 6.

In the following, results from coupled simulations are shown for a Hartmann number $Ha = 1000$, for which experiments have been performed [16]. For the 3-D simulations, a local coordinate system has been used in which the reference pressure has been chosen at the origin in the middle of the unit element and lengths are scaled with the mean Hartmann length a of the manifolds. The discussion of results starts with the case when the pressure drops along feeding and draining manifold channels are equal, i.e., when $\Delta p_f = \Delta p_d$. As a result we find different flow rates in both sub-channels, since the larger draining duct easily carries more flow ($\alpha_d = 0.605$) than the smaller feeding channel ($\alpha_f = 0.395$). Poloidal velocity profiles are shown in Fig. 3(a) for a position in the middle ($x = 0$) and at the entrance of the manifold part ($x = -2.1$). We observe slightly deformed core velocities with jets along the field-aligned walls. The figure further displays colored contours of electric potential plotted on the fluid-wall interface in one-half of the channels for $z > 0$, which shows, on one hand, the perturbations by the stiffening plate at $x = 0$ and the coupling along the baffle wall.

The influence of electromagnetic coupling becomes obvious when considering a flow that is driven only by a pressure difference Δp_f in the small feeding channel while the pressure difference in the draining duct is zero $\Delta p_d = 0$. Fig. 4 shows

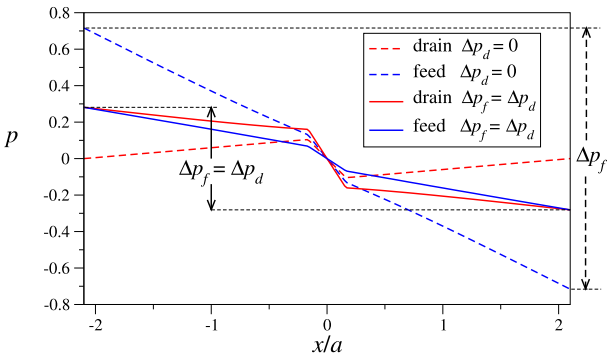

Fig. 5. Pressure distribution in a periodic fraction of the coupled manifolds along the scaled poloidal coordinate assuming the same pressure differences $\Delta p_f = \Delta p_d = 0.562$ in both ducts (solid lines) and results of a simulation where $\Delta p_f = 1.43$ and $\Delta p_d = 0$ (dashed lines).

such a result. Due to coupling by leakage current, the flow in the smaller feeding channel pulls the fluid in the neighboring draining duct in the same direction preferentially near the baffle wall. With increasing distance from the common wall, the velocity in the draining channel becomes smaller and at the walls parallel to **B** we observe even reverse jets.

The variation of pressure in the center of both manifolds is plotted for the two cases in Fig. 5 along the poloidal direction. The magnitudes of pressure drops in feeding and draining manifolds are indicated for $\Delta p_f = \Delta p_d = 0.562$ and for $\Delta p_f = 1.43$, $\Delta p_d = 0$. The figure shows smaller pressure gradients in the larger draining channel (solid red line) compared to those in the narrow feeding ducts (blue solid line) but larger 3-D effects are present near the stiffening plate where the changes in cross section are significant. The pressure drop in the feeding duct increases considerably when the flow in this channel also has to pull the one in the draining duct due to electromagnetic coupling. This can be seen in Fig. 5, where we observe reversed pressure gradients in the draining channel.

For a systematic analysis, a number of 3-D simulations have been performed and results are summarized in Fig. 6. The figure shows the relevant values of $\Delta p_f(\alpha_f)$ and $\Delta p_d(\alpha_d)$,

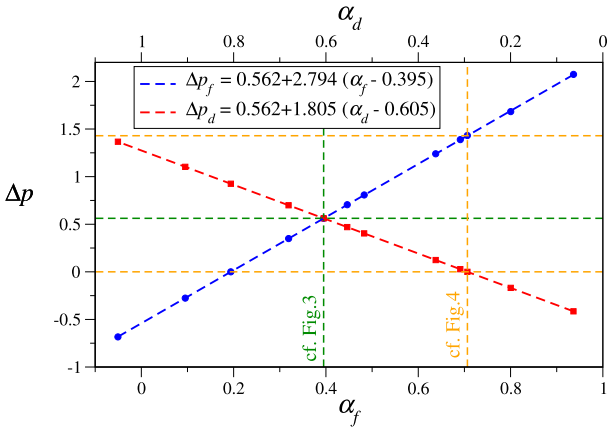

Fig. 6. Variation of pressure drops Δp_f and Δp_d with flow rate fraction α_f and α_d for manifolds according to the MHD mock-up with $e = 0.41$ derived from the WCLL-TBM design [8]. The data displayed by symbols has been obtained by coupled 3-D simulations of periodic manifold fractions, dashed blue and red lines represent linear fits.

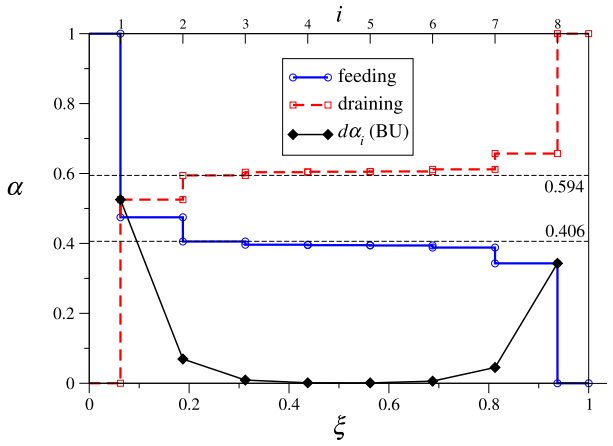

Fig. 7. Distribution of flow rates in feeding and draining channels of a WCLL TBM mock-up with manifolds according to the design in [8] with $e = 0.41$.

which are required for the global analysis in (4) and (5). The two special cases mentioned above in Figs. 3–5 correspond to the positions marked with vertical dashed lines at $\alpha_f = 0.395$ and $\alpha_f = 0.7065$, for which $\Delta p_f = \Delta p_d = 0.562$ and $\Delta p_f = 1.43$, $\Delta p_d = 0$, respectively. Another special flow configuration is $\alpha_f = 0.194$, for which the flow is exclusively driven by a pressure difference in the draining channel ($\Delta p_f = 0$). For using the data in the model (4)–(7), the numerical results have been approximated by analytical fits as shown by blue and red dashed lines and expressed as formulas in the legend of Fig. 6.

B. Global Analysis for Entire TBM

The iterative analysis for the entire TBM mock-up starts with assumed uniform initial distribution of flow rates $d\alpha_i$ in BUs. The pressure drop correlations used in the global model are those displayed in the legend of Fig. 6. Converged results obtained after a sufficiently large number of iterations are shown for flow rates in manifolds and BUs in Fig. 7 and for pressure distribution in manifolds in Fig. 8, respectively.

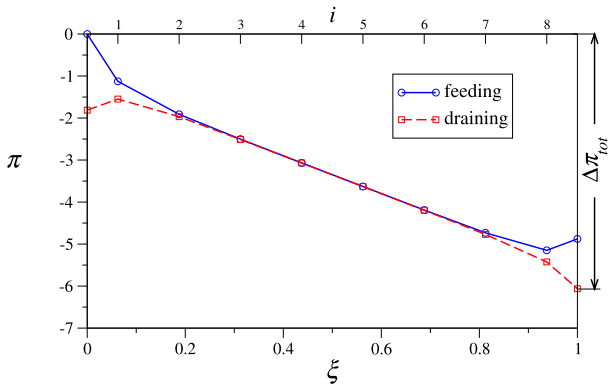

Fig. 8. Pressure distribution in feeding and draining manifolds in a WCLL TBM mock-up according to the design in [8] with $e = 0.41$. The related distribution of flow rates in BUs corresponds to the solid black line in Fig. 7.

Coming from the smaller feeding channel, the fluid tries to leap over to the larger draining duct as soon as possible. We observe in Fig. 7 that BU1 transfers approximately half of the flow from the feeding to the draining manifold channels. BU2 exchanges only 8%. Then the flow rate fractions are already close to $\alpha_f = 0.395$ and $\alpha_d = 0.605$ (Fig. 7), for which pressure drops in feeding and draining ducts are equal (Fig. 6) and the differences between feeding and draining pressure distributions in Fig. 8 almost disappear. Therefore, flow rates carried by BU3÷BU6 become insignificant. As a consequence, under such conditions, the fluid exchange in central BUs is not enforced, which would lead to accumulation of tritium in these "stagnant" units. The remaining flow is transferred to the draining duct via BU7 (5%) and BU8 (33%). The reason for the reduced flow in central BUs comes from the fact that the manifold geometry does not adjust to the flow rates carried by these channels, which had been identified already in previous references (e.g., [9] [4]). For the present work we may identify further a nonsymmetry of flow rates along the poloidal direction due to different size of feeding and draining channels with $e = 0.41 > 0$.

IV. Optimized Manifold for a WCLL-TBM

As shown above, BUs in the center of the module have strongly reduced flow rates compared to BUs close to both poloidal ends. In the present section an attempt is made to overcome this deficit in the design by positioning the separating baffle walls between both manifolds to optimized positions, i.e., to determine by analysis the best values for e depending on the poloidal position ξ. The procedure is based on analysis elements introduced in Sections II and III.

We have seen that a uniform flow partitioning in BUs can be expected only if the pressure differences between feeding and draining sections of manifolds are the same for all BUs, i.e., when $p_{f,i} - p_{d,i}$ are the same for all i (see e.g., 6). This can be ensured only when feeding and draining pressure distributions as shown, e.g., in Fig. 8 have constant distance to each other. Consequently for a manifold element of length dx it is required that $\Delta p_{f,i} = \Delta p_{d,i}$. The flow rate distributions $\alpha_{f,i}$ and $\alpha_{d,i}$ in feeding and draining ducts then adjust to satisfy the latter condition, depending on the position e of the

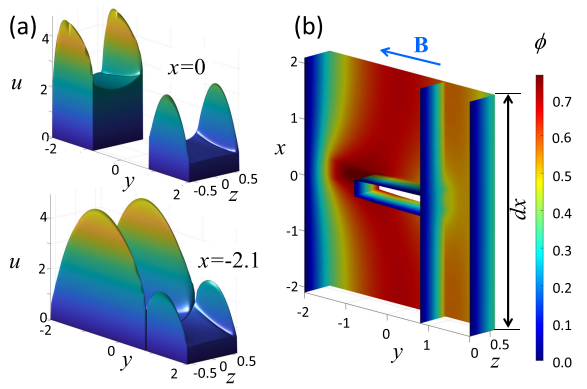

Fig. 9. Results of a simulation with electromagnetic coupling for pressure differences $\Delta p_d = \Delta p_f$ and $e = 0.8$, for which the baffle plate separating feeding and draining manifolds touches one end of the stiffening plate, which in general cases penetrates the separating wall reducing locally the cross sections of both ducts, i.e., for the present value $e = 0.8$, the feeding duct becomes straight. (a) Velocity profiles in the symmetry plane $x = 0$ and near the entrance $x = -2.1$ and (b) view on the distribution of nondimensional electric potential on the fluid-wall interface in half of the geometry.

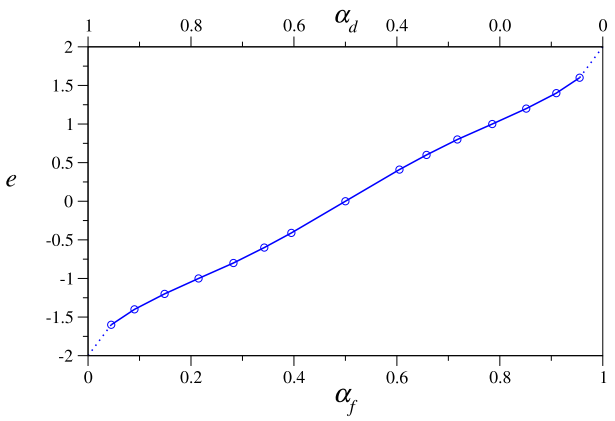

Fig. 10. Relation between position of baffle wall e and flow rate fractions α_f and $\alpha_d = 1 - \alpha_f$ obtained by 3-D coupled simulations with $\Delta p_f = \Delta p_d$.

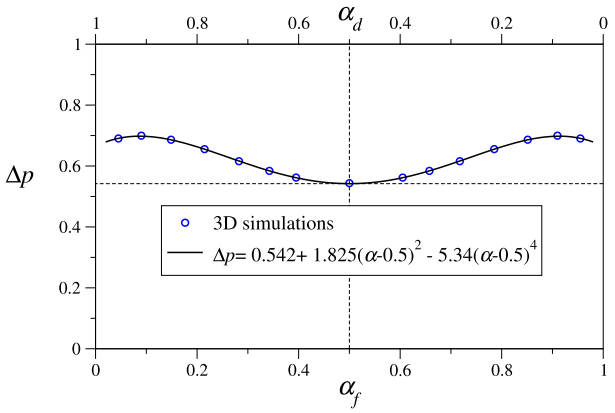

Fig. 11. Relation between magnitude of pressure drop and flow rate fractions α_f and $\alpha_d = 1 - \alpha_f$ obtained by 3-D coupled simulations with $\Delta p = \Delta p_f = \Delta p_d$ for simulations with $e(\alpha)$ according to Fig. 10. For the further evaluation of pressure drop and flow partitioning in the entire TBM mock-up using the manifold model, the analytical fitting function shown by the black line and expressed by the formula in the legend is used.

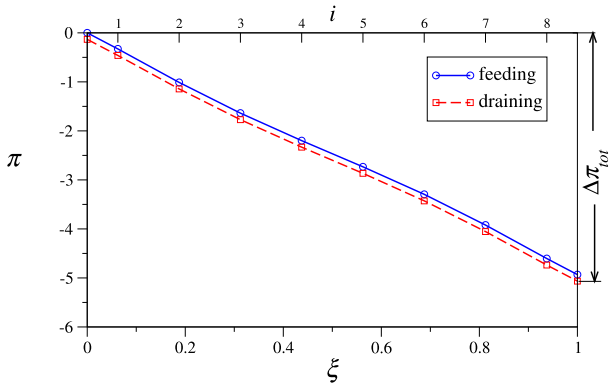

Fig. 12. Pressure distribution in feeding and draining manifolds in a WCLL TBM mock-up, where the positions of the baffle walls $e_i(\xi_i)$ have been optimized in order to achieve a uniform distribution of flow rates among all BUs.

baffle wall. Being aware of these constraints, a number of 3-D coupled simulations have been performed for assumed equal pressure heads in the feeding and draining sections, where in each simulation the position of the baffle wall e is varied as a parameter of the simulations. Results of one simulation of this type are shown in Fig. 9 for $e = 0.8$ from which it can be clearly seen that the wider manifold carries more flow.

As an outcome of a number of such simulations we identify for each value of e corresponding flow rate fractions α_f and α_d and the magnitude of pressure drops $\Delta p_f = \Delta p_d$. Results of these simulations are summarized and displayed in Figs. 10 and 11. It can be observed, that the position e determines essentially the distribution of flow rates in both manifolds, while the magnitude of pressure drop is only moderately affected (see Fig. 11). The dependence of pressure drop, determined in simulations as $\Delta p(e)$ plotted versus $\alpha_f(e)$ allows to define an analytical relation as a reasonable fitting function of data points in Fig. 11. With this information the remaining analysis is straightforward as outlined in (4) and (5) while in (6) the left-hand side is constant and determined by the a priori known flow rate distribution $d\alpha_i$.

With $\Delta p(\alpha)$ according to the legend shown in Fig. 11 we are now able to solve the problem (4) and (5) and determine the pressure and flow rate distribution in the manifolds. A result of a converged solution is shown in Fig. 12. We see that pressure distributions in feeding and draining manifolds now are equidistant which ensures uniform flow partitioning among all BUs. Moreover, as another positive side effect, it can be observed that with the optimized geometry, also the total pressure drop $\Delta\pi_{\text{tot}}$ is reduced from a value of $\Delta\pi_{\text{tot}} = 6.06$ (in Fig. 8) to a value of $\Delta\pi_{\text{tot}} = 5.07$ (in Fig. 12), i.e., by 16%.

It is worth to notice that with the present simulation model, it is not necessary to know the positions e_i of baffle plates when the calculations are started. The assumption of equal flow partitioning among BUs ($d\alpha_i = 1/N$) is enforced by the modeling. However, since we know how desired flow rates $\alpha_{f,i} = 1 - (i-1)d\alpha_i$ and $\alpha_{d,i} = (i-1)d\alpha_i$ in feeding and draining manifolds vary along poloidal direction ξ_i, it is possible to define for each geometric element i of length dx the optimum value of e_i according to the data displayed in Fig. 10. As a consequence the latter figure provides the required input for designing manifolds with best performance.

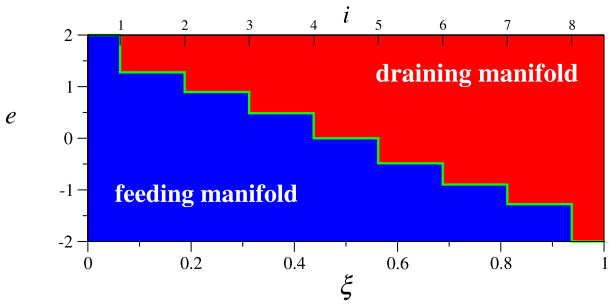

Fig. 13. Optimized position of the dividing baffle wall in the manifold for achieving uniform flow partitioning in all BUs.

A result of optimal positions of baffle walls e_i for the 8 BUs of the WCLL TBM mock-up is shown in Fig. 13.

V. Conclusion

The present work makes an attempt to quantify MHD pressure drop in feeding and draining manifolds of a WCLL TBM according to the existing design [8] and to determine the flow partitioning in BUs. The manifold is split along the poloidal direction into generic unit elements that are considered in detailed electrically coupled 3-D numerical analyses. In the latter simulations, full electric coupling of neighboring feeding and draining channels is taken into account as well as geometric constraints caused by stiffening plates that penetrate the manifolds. The purpose of 3-D simulations is to determine the pressure drops in feeding and draining parts, depending on the flow rate partitioning among these channels. These results are used later as input to iteratively compose a global solution to the problem.

As foreseen in the WCLL TBM design [8], the baffle walls have been placed in an asymmetric position. It turns out that in the central part of the module the pressure in feeding and draining ducts are nearly the same so that there exists practicality no driving pressure heads for central BUs $i = 3, 4, 5, 6$. As a consequence, the flow rates in these BUs remain negligibly small, while the flow is primarily exchanged via BUs near the ends of the module. This fact disqualifies the current design option for applications in ITER as already suggested in [4].

The derived model is very flexible and allows for efficient and fast determination of the electrically coupled MHD performance. Moreover, the theoretical model has been successfully applied to determine via the derived mathematical schemes the optimized positions of baffle walls that will guarantee a homogeneous flow partitioning among all BUs which is required for a good performance of the blanket concept. While the present model is capable of providing results for the overall behavior of the TBM with electrically coupled manifolds, further flow details, e.g., near the entrance or exist pipes or inside BUs have to be obtained from full numerical simulations of those components.

Acknowledgment

This work has been carried out within the framework of the EUROfusion Consortium, funded by the European Union via the Euratom Research and Training Programme (Grant Agreement No 101052200 — EUROfusion). Views and opinions expressed are however those of the author(s) only and do not necessarily reflect those of the European Union or the European Commission. Neither the European Union nor the European Commission can be held responsible for them.

References

[1] P. Arena et al., "Design and integration of the EU-DEMO water-cooled lead lithium breeding blanket," *Energies*, vol. 16, no. 4, p. 2069, Feb. 2023.
[2] L. Bühler, C. Mistrangelo, H.-J. Brinkmann, and C. Koehly, "Pressure distribution in MHD flows in an experimental test-section for a HCLL blanket," *Fusion Eng. Des.*, vol. 127, pp. 168–172, Feb. 2018.
[3] C. Mistrangelo and L. Bühler, "Determination of multichannel MHD velocity profiles from wall-potential measurements and numerical simulations," *Fusion Eng. Des.*, vol. 130, pp. 137–141, May 2018.
[4] C. Mistrangelo, L. Bühler, C. Koehly, and I. Ricapito, "Magnetohydrodynamic velocity and pressure drop in manifolds of a WCLL TBM," *Nucl. Fusion*, vol. 61, no. 9, Sep. 2021, Art. no. 096037.
[5] T. J. Rhodes, S. Smolentsev, and M. Abdou, "Magnetohydrodynamic pressure drop and flow balancing of liquid metal flow in a prototypic fusion blanket manifold," *Phys. Fluids*, vol. 30, no. 5, May 2018, Art. no. 057101.
[6] S. Smolentsev, "Physical background, computations and practical issues of the magnetohydrodynamic pressure drop in a fusion liquid metal blanket," *Fluids*, vol. 6, no. 3, p. 110, Mar. 2021.
[7] S. Siriano, F. R. Urgorri, A. Tassone, and G. Caruso, "3D MHD analysis of prototypical manifold for liquid metal blankets," *Nucl. Fusion*, vol. 63, no. 8, Aug. 2023, Art. no. 086005.
[8] J. Aubert et al., "Design and preliminary analyses of the new water cooled lithium lead TBM for ITER," *Fusion Eng. Des.*, vol. 160, Nov. 2020, Art. no. 111921.
[9] L. Bühler and C. Mistrangelo, "A simple MHD model for coupling poloidal manifolds to breeder units in liquid metal blankets," *Fusion Eng. Des.*, vol. 191, Jun. 2023, Art. no. 113552.
[10] C. Koehly, L. Bühler, and C. Courtessole, "Design of a scaled mockup of the WCLL TBM for MHD experiments in liquid metal manifolds and breeder units," *Fusion Eng. Des.*, vol. 192, Jul. 2023, Art. no. 113753.
[11] T. Batal, "Assembly of WCLL TBM: CAD product and parts (by CEA)," CEA, IRFM, Saint-Paul-lez-Durance, France, EUROfusion Project, Nov. 2019.
[12] O. J. Foust, *Sodium—NaK Engineering Handbook*. Paris, France: Gordon and Breach Science Publishers, 1972.
[13] *Stahl-Eisen-Werkstoffblatter*, Verlag Stahleisen Düsseldorf, 1992.
[14] L. Bühler and C. Mistrangelo, "Theoretical studies of MHD flows in support to HCLL design activities," *Fusion Eng. Des.*, vols. 109–111, pp. 1609–1613, Nov. 2016.
[15] L. Bühler, "Magnetohydrodynamic flows in abitrary geometries in strong, nonuniform magnetic fields," *Fusion Technol.*, vol. 27, pp. 3–24, Jan. 1995.
[16] C. Courtessole, H.-J. Brinkmann, L. Bühler, and J. Roth, "Experimental investigation of MHD flows in a WCLL TBM mock-up," in *Proc. 15th Int. Symp. Fusion Nucl. Technol.*, Las Palmas de Gran Canaria, Spain, Sep. 2023, pp. 10–15.

Leo Bühler received the Dr.-Ing. and habilitation degrees in fluid dynamics from the Karlsruhe Institute of Technology (KIT), Karlsruhe, Germany, in 1992 and 2008, respectively.

He is a Professor at the Department for Thermal Energy Technology and Safety at KIT and the Head of the MHD research group with MEKKA and MaPLE facilities. His research interests include any kind of MHD flow in generic and complex geometries, asymptotic analysis, code development, and validation through experiments.

Chiara Mistrangelo received the Ph.D. degree in fluid dynamics from the Karlsruhe Institute of Technology (KIT), Karlsruhe, Germany, in 2005.

She is a Senior Researcher and Lecturer at the Department for Thermal Energy Technology and Safety at KIT. Her current research interests include pressure driven and buoyancy driven convective MHD flows in complex geometries, code development, validation through experiments and benchmark activities.